ISSN 0036-0295, Russian Metallurgy (Metally), Vol. 2016, No. 2, pp. 124–130. © Pleiades Publishing, Ltd., 2016.
Original Russian Text © A.E. Galashev, V.A. Polukhin, 2016, published in Rasplavy, 2016, No. 2, pp. 123–134.

Computer Simulation of Heating of Nickel and Mercury on Graphene[1]

A. E. Galashev[a] and V. A. Polukhin[b, c]

[a] *Institute of High-Temperature Electrochemistry, Ural Branch, Russian Academy of Sciences, ul. Akademicheskaya 20, Yekaterinburg, 620219 Russia*
[b] *Ural Federal University, ul. Mira 19, Yekaterinburg, 620002 Russia*
[c] *Institute of Metallurgy, Ural Branch, Russian Academy of Sciences, ul. Amundsena 101, Yekaterinburg, 620016 Russia*
e-mail: pvalery@nm.ru

Received October 17, 2015; in final form, November 10, 2015

Abstract—The structural, kinetic, and adhesion properties of nickel and mercury films on two- and one-layer graphene are studied by molecular dynamics simulation upon heating to 3300 and 1100 K, respectively. Two-sided coating of graphene with nickel retards the flow of metal atoms over the surface at $T > 1800$ K. In the presence of mercury on graphene, Stone–Wales defects and the hydrated edges of the graphene sheet withstand an increase in the temperature up to 800 K. As the temperature increases, the Hg film coagulates into a drop.

DOI: 10.1134/S003602951602004X

INTRODUCTION

Single-layer graphene is a semimetal, has no band gap, and cannot be used an electronic device element. Two-layer graphene is a semiconductor; i.e., it has a band gap. Its properties depend on the rotation of graphene sheets with respect to each other, which can be performed by changing an electric field applied across the layers.

The most promising field of application of graphene is the creation of composite materials with metals, such as aluminum, copper, and nickel [1–4]. Here, nickel occupies a prominent place due to the possibility of its synthesis using graphene, mainly multilayer graphene. Nickel belongs to the materials that strongly interact with graphene. The chemical interaction between graphene and nickel takes place due to the hybridization of the *d* electrons of the metal and the π orbitals of graphene. As a result, the physical properties of graphene change significantly. The band gap in the electronic structure becomes open and the π band shifts to ~2 eV below the Fermi level. Ferromagnetic nickel imparts a magnetic moment to graphene. The changes in the electronic spectrum influence the dispersion of phonons, and a graphene monolayer on nickel does not produce a Raman spectrum.

Nickel can be used as a catalytic substrate with a high carbon solubility [5]. The formation of graphene on this substrate occurs in the following two stages: (i) dissolution of carbon in the metal and (ii) precipitation of graphene on the surface. Single-layer graphene can be synthesized on a smooth surface, and multilayer graphene or graphite can be grown on a terraced surface.

The authors of [6] proposed to use graphene-based composite membranes to assemble mercury. The structure and the physical properties of the liquid mercury/graphene interface have not yet been studied, and the prospects of application of graphene as a filter dictate the necessity of its investigation. Liquid mercury cannot wet graphite: mercury drops formed on highly ordered pyrolitic graphite has a contact angle of 152.5° [7]. Carbon nanotubes also cannot be wet with mercury, as with any liquid metal having surface tension γ higher than 0.18 N/m [8]. The surface tension of mercury is 0.46 N/m. Nevertheless, the internal space of a carbon nanotube can be wet and filled mercury via electrowetting [9].

The purpose of this work is to study the morphology and the change in the physical properties of the nickel and mercury films grown on perfect two-layer graphene and one-layer edge-hydrogenated graphene with a high concentration of Stone–Wales defects, respectively, during rapid heating.

COMPUTER MODEL

The calculations were performed by a classical molecular dynamics simulation. The following three types of empirical potentials describing interactions were used for the calculations: carbon–carbon (in graphene), metal–metal, and metal–carbon. The Tersoff potential [10, 11]

---

[1] Articles presented on 14 Russian conference "Structure and Properties of Metal and Slag Melts" (MIShR-14, September 21–25, 2015, Yekaterinburg).

$$U^{\mathrm{Ter}} = \frac{1}{2}\sum_{i}\sum_{j\neq i} f_c(r_{ij})\left\{f_R(r_{ij}) + b_{ij} f_A(r_{ij})\right\},\quad f_R(r) = A\exp(-\lambda_1 r),$$

$$f_c(r) = \begin{cases} 1, & r < R, \\ \dfrac{1}{2} + \dfrac{1}{2}\cos\dfrac{\pi(r-R)}{S-R}, & R < r < S, \\ 0 & r > S, \end{cases}\quad f_A(r) = -B\exp(-\lambda_2 r), \tag{1}$$

$$b_{ij} = \left(1 + \beta^n \varsigma_{ij}^n\right),\quad \varsigma_{ij} = \sum_{k\neq i,j} f_c(r_{ik}) g(\theta_{ijk}),\quad g(\theta) = 1 + \frac{c^2}{d^2} - \frac{c^2}{d^2 + (h - \cos\theta)^2},$$

was used as the base of representing the interactions in graphene. Here, subscripts i, j, and k designate carbon atoms; r_{ij} is the i–j bond length; and θ_{ijk} is the angle between bonds i–j and j–k. The parameters of Eq. (1) are taken from [11] except for parameter S.

This potential has to be modified for a two-dimensional (such as graphene) system with a covalent bond to be simulated [12]. In our model, the maximum coverage of covalent interaction (S) was increased from 0.21 to 0.23 nm. A very weak Lennard-Jones interaction with the parameters from [12], which have a character of attraction, was operative beyond the limits of covalent interaction. "Deceleration" at each atomic site of graphene at force $dV_{ij}(\Omega_{kijl})/dr_{ij}$, where torque potential $V_{ij}(\Omega_{kijl})$ was determined in [12], was applied to prevent the rotation of a graphene sheet.

The Ni–Ni interaction was represented by the Sutton–Chen potential [13]

$$U^{\mathrm{SC}} = \varepsilon\left[\frac{1}{2}\sum_{i}\sum_{j\neq i} V(r_{ij}) - c\sum_{i}\sqrt{\rho_i}\right], \tag{2}$$

where

$$V(r_{ij}) = \left(a/r_{ij}\right)^n,\quad \rho_i = \sum_{j\neq i}\left(a/r_{ij}\right)^m.$$

The parameters of potential U^{SC}: namely, ε, a, c, m, n, are given in [13]. The Ni–C interactions were set by the Morse potential with the parameters of the Ni(001)–graphene system presented in [14].

The following two systems are studied to analyze the stability of nickel films on perfect two-layer graphene (graphene-(2)): system I is a Ni film on graphene-(2), and system II is graphene-(2) coated with identical Ni films on either side. The calculations started at a temperature of 300 K. Every 1 mln time step, the temperature was increased by 500 K and the next calculation of the same time was performed. The last calculation corresponded to a temperature of 3300 K. The details of simulation of nickel and mercury films are similar and will be described below.

As a rule, pair potentials are used to simulate the Hg–Hg interaction, and the simplest potential among them is the Lennard-Jones (LJ) potential. The parameters of this potential were chosen according to the data on the viscosity of gaseous mercury [15].

The Silver–Goldman (SG) potential is adjusted to ab initio data and gives good agreement with the experimental results obtained for spectroscopic constants [16]. The SG potential is based on the Hartree–Fock dispersion model

$$V_{\mathrm{SG}}(r) = \exp(\alpha - \beta r - \gamma r^2) - f_c(r)\left(\sum_{n=3}^{5}\frac{C_{2n}}{r^{2n}}\right), \tag{3}$$

where

$$f_c(r) = \exp\left[-(1.28r_c/r - 1)^2\right],$$
$$r < 1.28r_c = 1.0,\quad r \geq 1.28r_c.$$

The potential parameters are given in [16].

The graphene–mercury interaction was described by the LJ potential with the parameters from [17]. Mercury was initially deposited onto graphene in the form of a film, since mercury wets glass, sapphire, and pyrolitic graphite under certain conditions. 50 Hg atoms were randomly deposited onto the graphene sheet made of 406 C atoms with six Stone–Wales defects. The system was initially balanced in an MD calculation with 200000 time steps $\Delta t = 0.2$ fs). The basic calculations were preformed from a temperature of 300 K. The system temperature was increased by 100 K every 10^6 time step. The end of calculation corresponded to a temperature of 1100 K. The equations of motion were solved by the Runge–Kutta method.

The hydrogenation of graphene creates small surface corrugation, which also increases the adhesion of the metal to graphene. The preliminary partial hydrogenation allowed us to harden graphene ribs and to stabilize bivacancies. An H atom is effectively added to every boundary C atom, including the vicinity of a bivacancy. More specifically, the entire CH group rather than individual H atoms were considered when interactions were taken into account. The LJ parameters of interactions between CH groups are given in [19]. The Lorentz–Berthelot rule was used to determine the LJ parameters of the C–CH interactions.

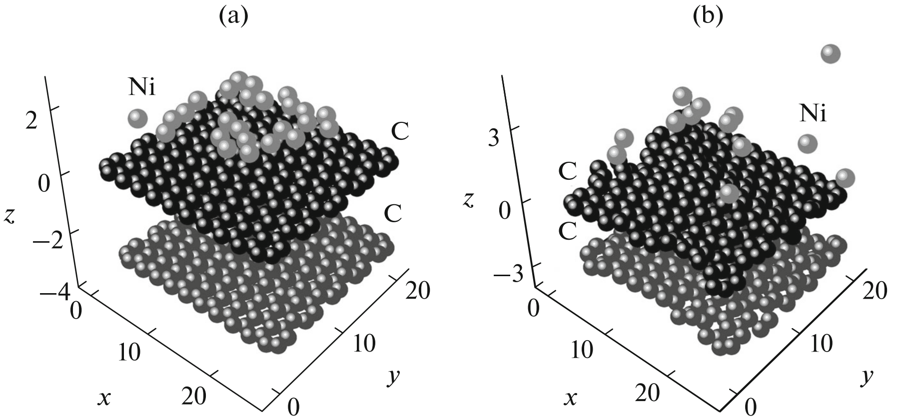

Fig. 1. Structure of two-layer graphene with a nickel film that corresponds to a time of 200 ps at a temperature of (a) 300 and (b) 3300 K. The atomic coordinates are given in angstroms.

The self-diffusion coefficient is determined in terms of the average metal atom displacement squared [20],

$$D = D_{xy} + D_z = \lim_{t\to\infty} \frac{1}{2\Gamma t}\left\langle [\Delta \mathbf{r}(t)]^2 \right\rangle, \tag{4}$$

where $\Gamma = 3$ is the space dimension, $\langle\ldots\rangle$ means time averaging and n is the number of time intervals used to determine $\left\langle [\Delta \mathbf{r}(t)]^2 \right\rangle$. Here, the time average was determined by averaging five curves calculated in a range of 40 ps (or 200000 Δt).

Contact angle θ between the mercury drop (film) surface and graphene was calculated by dividing the maximum horizontal section of the drop into the following three regions: (i) the circle of constant area that determines the area of contact with graphene, (ii) the ring that includes the projections of the neighbors nearest to region (i), and (iii) a similar ring to reveal external drop atoms. The Hg atoms nearest to the graphene surface were located in regions (i) and (ii). The parameters of searching for angle θ were empirically chosen. The averaging over the ring size and the heights of Hg atoms (or the number of chosen Hg atoms) in zones (ii) and (iii) gave average horizontal and vertical coordinates to find tgθ. Time averaging was used to determine angle θ.

The calculations were performed on the URAN hybrid cluster computer in the Institute of Mathematics and Mechanics, Ural Branch, Russian Academy of Sciences.

CALCULATION RESULTS

Figure 1 shows the configurations of the nickel–graphene-(2) system with one-sided coating of graphene with the metal that belong to a time of 200 ps and temperatures of 300 and 3300 K. At 300 K, Ni atoms coagulate into a dense two-dimensional “drop.” Both graphene sheets retain a regular hexagonal cellular structure at this temperature. At 3300 K, the vertices of the sheets bulge. Atomic disordering takes place in the vicinity of the sheet edges and C atoms do not leave the sheets. At 3300 K, more than half the Ni atoms evaporated.

Figure 2 shows the radial distribution functions $g(r)_{\text{Ni–Ni}}$, plotted for the Ni atom that is nearest to the centers of the upper and lower graphene sheets at T = 300 K. The Ni atoms on the upper sheet form a compact group, which is indicated by the high first peak and the rather high second peak (other peaks are weak). The Ni atoms on the lower graphene sheet are much more uniformly distributed. Four peaks (with subpeaks) are clearly visible here, and the intensity of the first peak is substantially lower (by a factor of 2.5). On the whole, the shapes of these functions point to different atomic arrangement with respect to the small central region in the upper and lower sheets. The lower sheet is much weakly deformed than the upper sheet, which is related to the fact that Ni atoms leave it faster.

Figure 3 depicts the kinetics of Ni atoms on the surface of graphene-(2). It is seen that the mobility of Ni atoms in horizontal directions D_{xy} for system I first decreases up to a temperature of 1800 K and then increases sharply (Fig. 3a). The initial decrease in coefficient D_{xy} is related to the enhancement of the adhesion of Ni atoms to the graphene substrate up to a certain threshold temperature. The second cause of this decrease is the densification of the nickel film on graphene, which occurs due to the discrepancy between the initial Ni density and the density in the condensed state. The experimental melting temperature of nickel is T_{m} = 1726 K. Therefore, the further increase in the temperature (above 1800 K) is most likely to cause melting of the film and the related increase in mobility D_{xy}. At T > 2300 K, D_{xy} of the

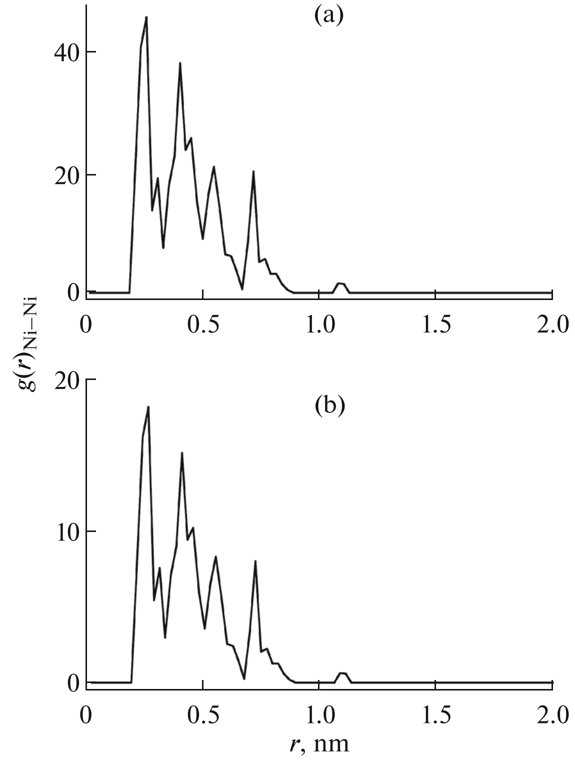

Fig. 2. Radial distribution functions for nickel films on graphene at $T = 300$ K: (a) upper and (b) lower Ni films.

one-sided Ni film continues to grow with temperature and this growth is moderate. Coefficient D_{xy} for the nickel films of system II behaves differently. In this case, D_{xy} increases almost monotonically with temperature, which is characteristic of both the upper and lower Ni films. This behavior of D_{xy} is explained by predominant strong Ni–Ni interactions between atoms in a film as compared to the analogous interactions between the metallic atoms belonging to different films and to Ni–C interactions. Note that D_{xy} in the upper Ni film is substantially lower than D_{xy} of the lower film at all temperatures.

Components D_z of the mobility of Ni atoms in the vertical direction also behave differently in systems I and II when temperature increases (Fig. 3b). Coefficient D_z in system I retains a stable low value up to a temperature of 1800 K. At higher temperatures, D_z of Ni atoms in this system increases sharply. Such a sharp increase in D_z is absent in system II. Here, coefficient D_z of Ni atoms first increases insignificantly (to a temperature of 1800 K for the upper Ni film and to $T =$ 1300 K for the lower film) and then oscillates, slightly increasing at a temperature of 3300 K. The substantial increase in coefficient D_z in system I at $T > 1800$ K is caused by the evaporation of some Ni atoms from the graphene sheet surface, which occurs predominantly straight up [21, 22]. The interaction of the Ni atoms belonging to different films restricts this process in system II. Here, the Ni atoms that leave the graphene surface have higher horizontal velocity components.

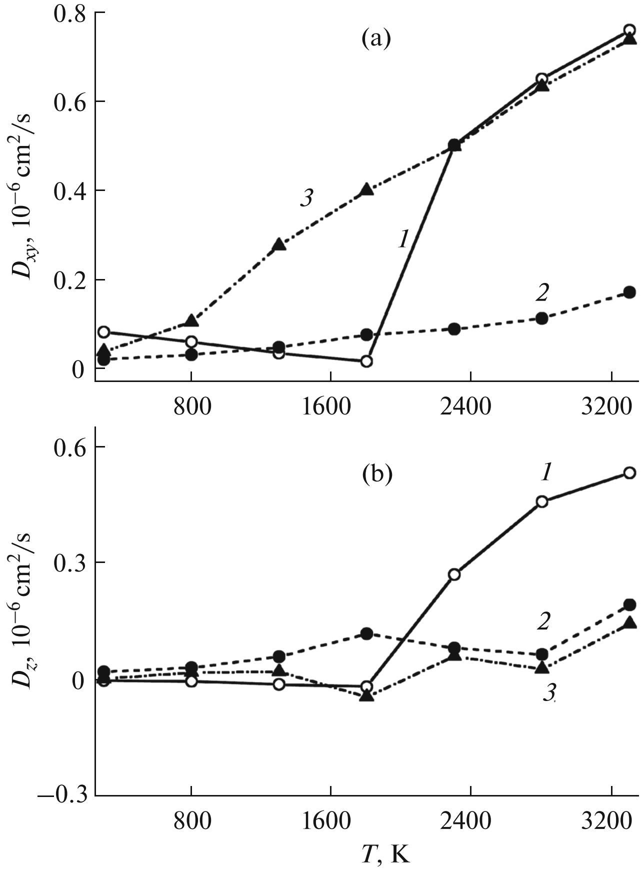

Fig. 3. Self-diffusion coefficient of nickel atoms in (a) horizontal plane and (b) vertical direction: (*1*) one top Ni film on two-layer graphene and (*2*) upper and (*3*) lower Ni films on two-layer graphene coated on both sides.

Figure 4 shows the changes that occur in the mercury film on graphene upon heating. The liquid metal film begins to separate out from graphene at $T =$ 300 K, which manifests itself in rising the edges of the film over graphene and its thickening. Atoms from the central part of the bent Hg film are more strongly bound to the substrate and have an average minimum distance $\bar{r}_{\text{C–Hg}}^{\min} = 0.28$ nm, which is created by 12–18 atoms. At a temperature of 600 K, the Hg film finally transforms into a drop, which is in contact with graphene. In this case, the average distance increases to $\bar{r}_{\text{C–Hg}}^{\min} = 0.34$ nm. The further increase in the temperature results in rising the drop mass above the graphene surface. At 1100 K, the average distance is $\bar{r}_{\text{C–Hg}}^{\min} = 0.47$ nm.

The radial distribution functions $g(r)$, of the Hg atom nearest to the center of the liquid mercury mass

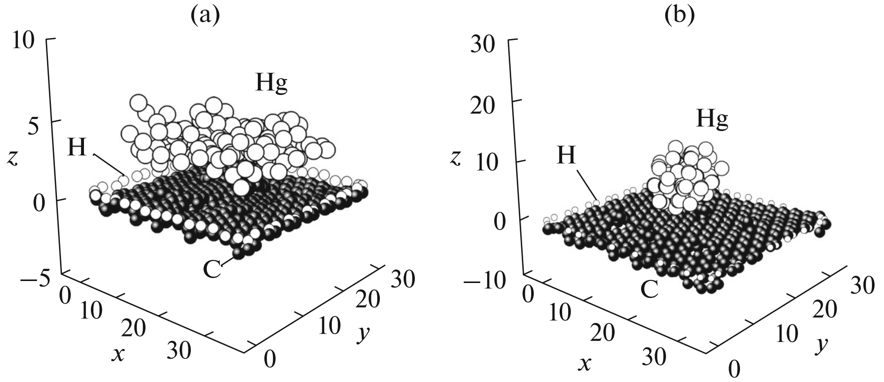

Fig. 4. Configurations of the system consisting of an Hg film on partly hydrated imperfect graphene that were obtained upon step-like heating at a temperature of (a) 300 and (b) 1100 K. The atomic coordinates are given in angstroms.

also indicate the formation of a more compact structure at $T = 1100$ K than at 300 K (Fig. 5). Function $g(r)$, reflects the spherically averaged structure of liquid mercury. The decrease in the number of peaks of function $g(r)$, at $T = 1100$ K evidences the formation of an irregular compact structure, where the distance to the nearest neighbors is estimated to be $r_1 = 0.29$ nm and the distance to the next-nearest neighbors is $r_2 = 0.48$–0.57 nm. The experimental values of these quantities for liquid mercury at 300 K are $r_1 = 0.31$ nm and $r_2 = 0.59$ nm [23].

When the Hg coagulates into a drop, horizontal mobility component D_{xy} of mercury atoms decreases and vertical component D_z passes through a minimum at a temperature of 600 K (Fig. 6). The smooth decrease in D_{xy} characterizes the coagulation of the film into a dense drop. The behavior of D_z indicates that drop formation ends at $T = 600$ K and that the further increase in temperature slightly enhances the vertical mobility due to an insignificant increase in the distance between the drop and the graphene surface.

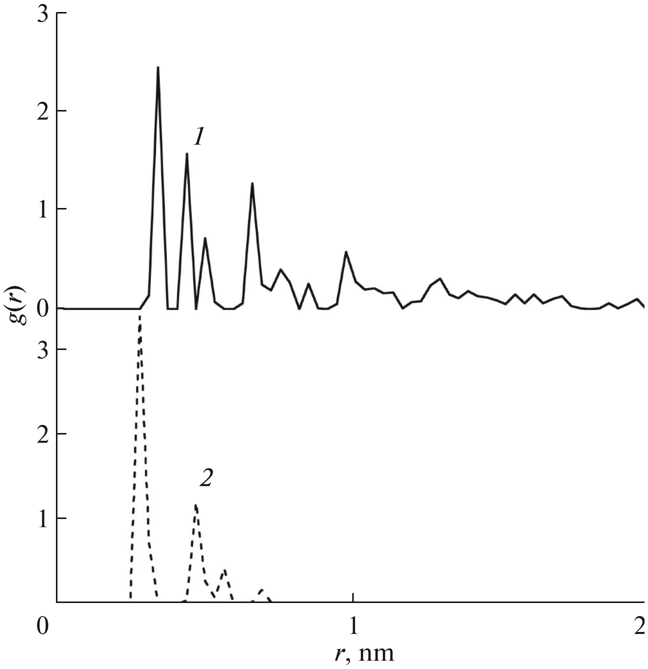

Fig. 5. Radial distribution functions of liquid mercury on graphene calculated at a temperature of (*1*) 300 and (*2*) 1100 K.

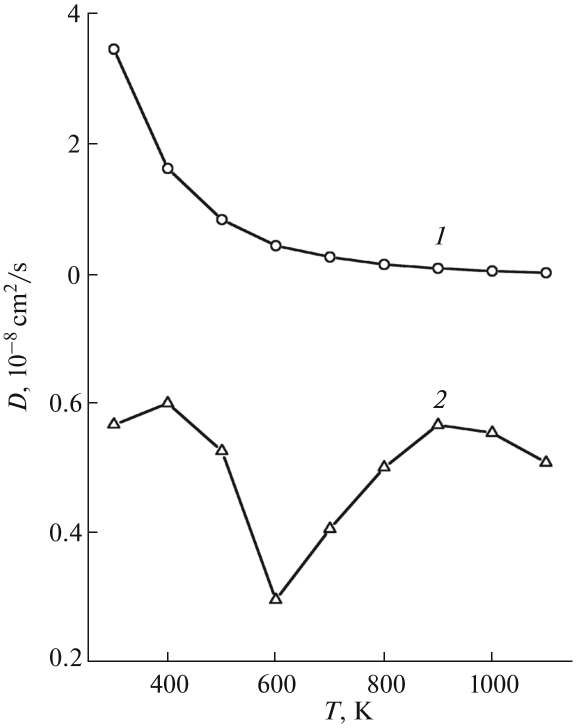

Fig. 6. (*1*) Horizontal and (*2*) vertical components of the mobility of Hg atoms obtained upon heating of liquid mercury on graphene.

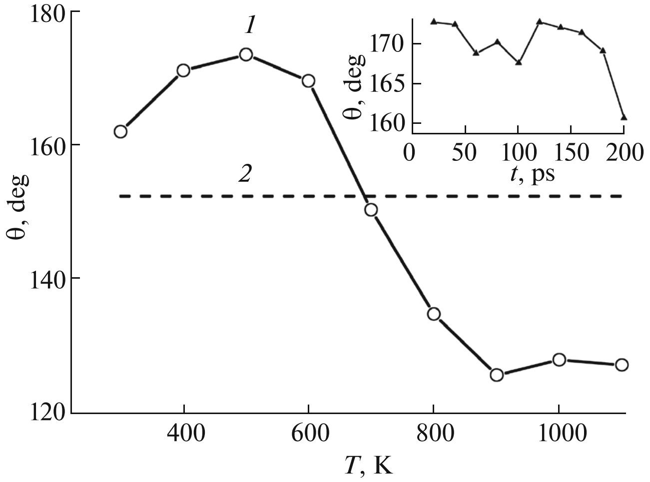

Fig. 7. (*1*) Contact angle of a mercury drop on graphene at various temperatures and (*2*) contact angle for a mercury droplet on pyrolitic graphite [7]. (inset) Time dependence of the contact angle of a mercury drop on graphene at $T = 600$ K.

The change in the wettability during the coagulation of the mercury film into a drop can be traced from the temperature dependence of calculated contact angle θ (Fig. 7). As temperature increases, the obtuse contact angle of the drop becomes closer to the flat angle. Despite noticeable rising of the drop above graphene, which begins at a temperature of 600 K, the separation of the drop from the substrate can only be attributed to a temperature of 800 K. The average angle corresponding to 900–1100 K $\overline{\theta} = 127.1°$ can be considered as the contact angle of a 100-atom Hg cluster on graphene. This angle is significantly lower than the contact angle of a mercury droplet on pyrolitic graphite (Fig. 7, dashed line) [7]. This behavior agrees with the generally accepted concepts of a decrease in angle θ when the drop radius decreases. The inset to Fig. 7 shows the time dependence of angle θ at a temperature of 600 K. Angle θ is seen to decrease noticeably at the end of calculation at this temperature.

CONCLUSIONS

A molecular dynamics simulation was used to study the behavior of monoatomic nickel films on graphene-(2) upon heating from 300 to 3300 K. The presence of the second graphene sheet significantly enhances the resistance of the planar hexagonal cellular structure to heating. When the system is heated, the nickel film is destroyed. However, even at $T = 3300$ K, some Ni atoms are retained on the upper graphene sheet irrespective of whether the lower sheet was preliminarily coated with the metal. The lower graphene sheet loses all Ni atoms at a temperature of 3300 K. The temperature dependences of the horizontal and vertical components of the self-diffusion coefficient of Ni atoms have a pronounced inflection point at $T = 1800$ K in the case of coating of graphene-(2) with a metal film on one side. However, when metal films are deposited on both sides, dependence $D_{xy}(T)$ increases monotonically for each coating, and $D_{xy}(T)$ of the lower Ni film is significantly higher than that of the upper film. The $D_z(T)$ dependences for the upper and lower nickel films have an insignificant inflection point at $T = 1800$ K.

A graphene sheet covered with a mercury film and having a high concentration of Stone–Wales defects was studied. The edges of the sheet were hydrated. An increase in the temperature led to gradual coagulation of the film into a drop and slow separation of the drop from graphene. The formation of a mercury drop is accompanied by a decrease in the domain of a radial distribution function, the number of pronounced $g(r)$ peaks, and their intensities. The horizontal component of the mobility of Hg atoms decreased gradually during this process, and the vertical component increased nonmonotonically after the decrease reached to a temperature of 600 K. An increase in temperature accelerates the formation of a drop and decreases the contact angle of the drop.

Thus, the presence of Ni films on both sides of graphene-(2) creates a stabilizing effect for Ni atoms to be held on graphene. Upon rapid heating, the mercury film on graphene transforms into a drop, which is accompanied by a substantial change in the atomic packing and the physical properties.

ACKNOWLEDGMENTS

This work was supported by the government of the Russian Federation (decision no. 211, contract no. 02.A03.21.0006) and by the Russian Foundation for Basic Research (project no. 13-08-00273).

REFERENCES

1. A. E. Galashev and V. A. Polukhin, "Computer study of the physical properties of a copper film on a heated graphene surface," Physics of the Solid State **55** (8), 1733–1738 (2001).
2. A. E. Galashev and V. A. Polukhin, "Removal of copper from graphene by bombardment with argon clusters: computer experiment," Physics of Metals and Metallography **115** (7), 697–704 (2014).
3. A. E. Galashev, "Computer stability tests for aluminum films heated on a graphene sheet," Tech. Phys. **59** (4), 467–473 (2014).
4. A. E. Galashev and O. R. Rakhmanova, "Stability of graphene and the materials based on it during mechanical and thermal actions," Usp. Fiz. Nauk **184** (10), 1045–1065 (2014).
5. V. A. Polukhin and N. A. Vatolin, "Stability and thermal evolution of transition metal and silicon clusters," Russ. Chem. Rev. **84** (5), 498–539 (2015).
6. R. Li, L. Liu, and F. Yang, "Preparation of polyaniline/reduced graphene oxide nanocomposite and its

application in adsorption of aqueous Hg(II)," Chem. Eng. J. **229**, 460–468 (2013).

7. A. Awasthi, Y. J. Bhatt, and S. P. Garg, "Measurement of contact angle in systems involving liquid metals," Meas. Sci. Technol. **7**, 753–757 (1996).
8. E. Dujardin, T. W. Ebbesen, H. Hiura, and K. Tanigaki, "Capillarity and wetting of carbon nanotubes," Science **265**, 1850–1851 (1994).
9. J. Y. Chen, A. Kutana, C. P. Collier, and K. P. Giapis, "Electrowetting in carbon nanotubes," Science **310**, 1480–1483 (2005).
10. J. Tersoff, "New empirical approach for the structure and energy of covalent systems," Phys. Rev. B: Condens. Matter **37**, 6991–7000 (1988).
11. J. Tersoff, "Modeling solid-state chemistry: interatomic potentials for multicomponent systems," Phys. Rev. B: Condens. Matter **39**, 5566–5568 (1988).
12. S. J. Stuart, A. V. Tutein, and J. A. Harrison, "A reactive potential for hydrocarbons with intermolecular interactions," J. Chem. Phys. **112**, 6472–6486 (2000).
13. H. Rafii-Tabar, "Modeling the nano-scale phenomena in condensed matter physics via computer-based numerical simulations," Physics Reports **325**, 239–310 (2000).
14. M. Moseler, F. Cervantes, S. Hofmann, G. Csanyi, and A. C. Ferrari, "Origin of the quasi-solid state of catalyst nanoparticles in growing nanotubes and nanofibers," ACS Nano **4**, 7587–7595 (2010).
15. F. Epstein and M. D. Powers, "Liquid metals. I. The viscosity of mercury vapor and the potential function for mercury," J. Phys. Chem. **57**, 336–341 (1953).
16. L. J. Munro and J. K. Johnson, "An interatomic potential for mercury dimer," J. Chem. Phys. **114**, 5545–5551 (2001).
17. A. Kutana and K. P. Giapis, "Atomistic simulations of electrowetting in carbon nanotubes," Nano Lett. **6**, 656–661 (2006).
18. P. Schwerdtfeger, R. Wesendrup, G. E. Moyano, A. J. Sadlej, J. Greif, and F. Hensel, "The potential energy curve and dipole polarizability tensor of mercury dimer," J. Chem. Phys. **115**, 7401–7412 (2001).
19. F. D. Lamari and D. Levesque, "Hydrogen adsorption on functionalized graphene," Carbon **49**, 5196–5200 (2011).
20. A. E. Galashev and A. A. Galashev, "Computer simulation of the cluster bombardment of a lead film on graphene," Khim. Vys. Energ. **49** (2), 135–140 (2015).
21. V. A. Polukhin and E. D. Kurbanova, "Dependence of the thermal stability of the interface states of *d* metals (Cu, Pd, Ti, Ni) and Al with graphene on the character of sorption and diffusion mobility in a contact zone," Russ. J. Chem. Phys. **3**, 1–18 (2015).
22. V. A. Polukhin, E. D. Kurbanova, and A. E. Galashev, "Comparative analysis of termoscale effects, isomerization and stability of TM-nanoclusters (Pd, Ni, Fe) and Si in dependence on interatomic potentials. MD-simulations," EPJ Web of Conferences **15**, 030021–030025 (2011).
23. R. V. G. Rao and A. K. K. Murthy, "Mean spherical model and structure factor of liquid mercury and aluminium," Phys. Stat. Sol. **66**, 703–707 (1974).

Translated by K. Shakhlevich